Journal of Geophysical Research: Atmospheres

RESEARCH ARTICLE
10.1029/2018JD029262

Evaluating Climate Sensitivity to CO_2 Across Earth's History

E. T. Wolf[1,2], J. Haqq-Misra[2,3], and O. B. Toon[1]

[1]Laboratory for Atmospheric and Space Physics, Department of Atmospheric and Oceanic Sciences, University of Colorado Boulder, Boulder, CO, USA, [2]NASA Astrobiology Institute's Virtual Planetary Laboratory, Seattle, WA, USA, [3]Blue Marble Space Institute of Science, Seattle, WA, USA

Key Points:
- Climate sensitivity to CO_2 varied significantly across Earth's history
- The adjusted radiative forcing from CO_2 increases at high concentrations
- Cloud albedo feedback cause an abrupt transition in climate for warming atmospheres

Correspondence to:
E. T. Wolf,
eric.wolf@colorado.edu

Citation:
Wolf, E. T., Haqq-Misra, J., & Toon, O. B. (2018). Evaluating climate sensitivity to CO_2 across Earth's history. *Journal of Geophysical Research: Atmospheres*, *123*. https://doi.org/10.1029/2018JD029262

Received 26 JUN 2018
Accepted 17 OCT 2018
Accepted article online 22 OCT 2018

Abstract CO_2-driven changes to climate have occurred during many epochs of Earth's history when the solar insolation, atmospheric CO_2 concentration, and surface temperature of the planet were all significantly different than today. Each of these aspects affects the implied radiative forcings, climate feedbacks, and resultant changes in global mean surface temperature. Here we use a three-dimensional climate system model to study the effects of increasing CO_2 on Earth's climate, across many orders of magnitude of variation, and under solar inputs relevant for paleo, present, and future Earth scenarios. We find that the change in global mean surface temperature from doubling CO_2 (i.e., the equilibrium climate sensitivity) may vary between 2.6 and 21.6 K over the course of Earth's history. In agreement with previous studies, we find that the adjusted radiative forcing from doubling CO_2 increases at high concentrations up to about 1.5 bars partial pressure, generally resulting in larger changes in the surface temperature. We also find that the cloud albedo feedback causes an abrupt transition in climate for warming atmospheres that depends both on the mean surface temperature and the total solar insolation. Climate sensitivity to atmospheric CO_2 has probably varied considerably across Earth's history.

Plain Language Summary It is evident that climate sensitivity to changing CO_2 varies if the amount of solar energy received by Earth is different, if the starting CO_2 amount is different, or if the mean temperature of the planet is significantly different.

1. Introduction

The magnitude of the response of surface temperatures to changing CO_2 is a central question of climate science. Of immediate concern, climate change caused by anthropogenic CO_2 emissions threatens to induce several degrees of warming by the end of the century (IPCC, 2014). Of general concern, the regulation of CO_2 by the carbonate–silicate cycle has played a central role in modulating climate over the entirety of Earth's history (Kasting, 1987). Meanwhile, the Sun has increased in brightness by ~25% over the course of Earth's history and will continue to brighten into the future, following a standard stellar evolutionary path for main sequence stars (Gough, 1981; Ribas, 2009). In light of the faint young Sun, a warm early Earth (as is observed in the geologic record) is typically attributed to high levels of CO_2 in the atmosphere sourced from intense early volcanism (Charnay et al., 2013; Haqq-Misra et al., 2008; Kasting, 1987; Wolf & Toon, 2013; Wolf & Toon, 2014). Geologic evidence from paleo-CO_2 indicators also supports larger atmospheric CO_2 in the distant past, which has subsequently been drawn down slowly over time (Driese et al., 2011; Hessler et al., 2004; Rye et al., 1995; Sheldon, 2006). The Earth's temperature throughout history has largely been stabilized by the negative feedback that exists between atmospheric CO_2, surface temperature, and weathering rates, through the action of the carbon-silicate cycle (Walker et al., 1981). Still, significant excursions in CO_2 concentrations are believed to be responsible for both entrance and egress from snowball Earth events (Hoffman et al., 1998; Pierrehumbert et al., 2011), and for warm periods in the paleoclimate record such as the Palocene-Eocene thermal maximum (Kennett & Stott, 1991; Koch et al., 1992) or the Permian–Triassic boundary (Kidder & Worsley, 2004). Estimates of deep-paleoclimate temperatures vary wildly, ranging possibly as high as ~340 K (Knauth & Lowe, 2003; Robert & Chaussidon, 2006), implying that a strong greenhouse effect may have occurred on the early Earth. Even more conservative estimates place paleotemperatures during the Archean above 300 K (Blake et al., 2010; Hren et al., 2009), requiring CO_2 levels significantly higher than that of the present-day Earth. While many factors including continental positioning (Poulsen et al., 2002), modulation of ocean heat transports (Donnadieu et al., 2004), prevalence of cloud condensation nuclei (Rosing et al., 2010), and background N_2 amount (Goldblatt et al., 2009), can affect climate changes, still, the

combined effects of greenhouse and solar forcings determine a planet's energy balance and thus climate to first order (Budyko, 1969).

In general, radiatively important changes to atmospheric CO_2 concentrations can occur on time scales that are significantly shorter than the rate of the brightening Sun. Every ~110 million years, the Sun brightens by ~1%, equivalent to an ~3.4 W/m^2 top-of-atmosphere radiative forcing (Schroder & Smith, 2008). However, the *e*-folding time scale of atmospheric CO_2 due to carbon-silicate cycling is only few hundred thousand years (Sundquist, 1991). Note that a factor of two change in atmospheric CO_2 from present levels causes a 3–4 W/m^2 radiative forcing (Forster et al., 2013), which is thus equivalent to about a 1% change in the solar constant. The near-term paleoclimate record derived from Vostok ice cores confirms that variability in paleotemperatures mirrors the variability in paleoatmospheric CO_2 (Petit et al., 1999). Thus, it is reasonable to conclude that changes to atmospheric CO_2 have acted as a significant driver of climate change over the age of the Earth.

The response of climate to changing atmospheric CO_2 can perhaps be most simply characterized in terms of the equilibrium climate sensitivity (ECS; IPCC, 1990). ECS is the change in global mean surface air temperature (T_s) that results from doubling the atmospheric CO_2 concentration and allowing the climate to reach a new equilibrium. ECS is commonly determined from 3-D climate model simulations, with an instantaneously imposed step-forcing for CO_2. ECS considers the effects of the implied radiative forcing and decadal scale climate feedbacks including changes to clouds, water vapor, snow and ice coverage, and lapse rate. However, processes that operate on geologic time scales, such as changes in the position of continents, land glaciers, and variations in Earth's orbital obliquity, are not considered in ECS. Thus ECS described in this work considers only so-called fast-feedbacks and is also commonly referred to in the literature as the Charney sensitivity (Charney, 1979). Note that ECS (units of K) is different from specific climate sensitivity (units of K $(W/m^2)^{-1}$). While ECS is easily grasped, it masks whether changes in temperature are driven by radiative forcings or by climate feedbacks. On the other hand, specific climate sensitivity is the change in mean surface temperature for a unit of radiative forcing, and thus isolates the effect of climate feedbacks. Caballero and Huber (2013) showed using a similar model to ours that both the radiative forcing and the specific climate sensitivity increase for the first several doublings of CO_2 beyond the preindustrial level.

Based on a large collection of 3-D climate system model simulations from many groups, the IPCC Fifth Assessment Report (IPCC, 2014) estimates that a doubling of CO_2 from present-day conditions would cause Earth to warm by 1.5–4.5 K. Likewise, Rogelj et al. (2012) estimates ECS be to be about 3 K based on the synthesis of observational and modeling studies. However, these estimates for ECS are valid only for a single set of initial conditions (i.e., the present-day Earth), and are not necessarily useful for considering larger CO_2 forcings, or Earth at different periods in its history, or in a different initial climate state. The total solar insolation, atmospheric CO_2 concentration, and the initial state (i.e., mean temperature) of the atmosphere have varied considerably over the course of Earth's history. There is little reason to expect that the sensitivity of climate to CO_2 has remained constant over such a wide range of conditions and radiative forcings. Indeed, some recent calculations predict that ECS may increase for the next several CO_2 doublings beyond the present day (Caballero & Huber, 2013; Hansen et al., 2005; Meraner et al., 2013; Russell et al., 2013).

Here we use a 3-D climate system model to study the sensitivity of Earth's climate to large variations in atmospheric CO_2. We study paleo-Earth under a weak Sun, future Earth under a bright Sun, and the present day. We find that the sensitivity of climate to CO_2 varies considerably, owing to increasing radiative forcing from CO_2 at high concentrations, and to nonlinear feedbacks in the cloud albedo that depend on the total solar insolation and surface temperature. The remainder of the paper is organized as follows: In section 2, we describe our climate model and procedures. In section 3, we discuss steady state climate solutions and the resultant equilibrium climate sensitivities. In section 4, we use Gregory analysis (Gregory et al., 2004) to differentiate climate forcings and feedbacks. In section 5, we discuss the role of cloud feedback. In section 6, we discuss the ramifications of our results, and we conclude the work in section 7.

2. Model Description

We use an identical model configuration as in Wolf and Toon (2015), which studied the warming of Earth's climate under increasing solar insolation. We use a modified version of the Community Earth System

Model (CESM) version 1.2 from the National Center for Atmospheric Research. We utilize the Community Atmosphere Model version 4 (Neale et al., 2010), with 4° × 5° horizontal resolution and 45 vertical levels extending to an ~0.2 mb model top and with a finite volume dynamical core (Lin & Rood, 1996). Note that the CAM4 finite volume core is prone to spurious angular momentum errors; however, the inclusion of realistic topography minimizes these errors in Earth simulations (Lebonnois et al., 2012). We use present-day Earth continents, topography, and land surface, except that permanent land glaciers over Antarctica and Greenland have been replaced with bare soil. However, snow cover and sea ice can accumulate and build where conditions are sufficiently cold. Note that our control simulations, and also prior modeling work by others (Goldner et al., 2014, 2013), suggest that removing permanent ice sheets has a relatively small overall impact on global mean climate. We have modified the radiative transfer code to simulate high-CO_2 atmospheres (Wolf & Toon, 2013). Orbital-rotational parameters (obliquity, rotation rate, eccentricity, and length of year) and the wavelength dependence of the incident solar spectrum are also held identical to the present-day Earth. We use a thermodynamic slab ocean model of 50-m depth with prescribed "*q*-flux" ocean heat transport terms that mimic present-day ocean heat transport (Bitz et al., 2012). Simulations are run for 50 to 75 model years, with most taking 20 to 30 model years to reach a statistical steady state. Note that prior works demonstrate that the ECS for one doubling of CO_2 is about the same for CESM run with either *q*-flux or a fully dynamical ocean model (Bitz et al., 2012; Danabasoglu & Gent, 2009). For warming climates, as are studied here, changes in ocean heat transport are thought to impact climate mainly through feedbacks involving deep convection, clouds, and water vapor within midlatitude storm tracks, as opposed to changes in magnitude and location of the total poleward heat transport (Rose & Ferreira, 2013).

We assume a 1-bar N_2 background, with the addition of CO_2 in fixed amounts, and variable water vapor determined by the Clausius-Clapeyron relation and the availability of water. The total pressure of the atmosphere equals the sum of partial pressures of N_2, CO_2, and H_2O gases. Note that for high-CO_2 simulations, the total surface pressure grows significantly larger than that of the present-day Earth. Pressure broadening continua are included using the MT_CKD model (Clough et al., 2005). CO_2 self-broadening is taken to be 1.3 times the foreign-broadening component. H_2O foreign broadening is assumed to be from Earth-air. Our method follows the "MTCKD" parameterization described in Halevy et al. (2009), and at high-CO_2 produces intermediate-strength absorption compared to other popular CO_2 continuum parameterizations (Halevy et al., 2009). In order to simplify these calculations we have ignored the formation of stratospheric ozone and the presence of oxygen in the atmosphere. Ozone is a minor greenhouse gas, and oxygen impacts the radiation balance and surface temperatures only slightly. Without ozone our simulations lack a stratospheric inversion, which raises the height of the tropopause and permits cold stratospheric temperatures and optically thin high-altitude cirrus cloud decks (e.g., Wolf & Toon, 2013, 2015). Note that Earth was largely anoxic prior to ~2.45 Ga, before jumping to perhaps several percent of the atmosphere and higher at later times (Holland, 2006). Furthermore, for warm moist climates, catalytic cycles involving hydroxyl radicals may be expected to destroy stratospheric ozone (Kasting & Donahue, 1980; Lary, 1997). All simulations are initiated from present-day global mean surface temperatures. We limit our study to climates warmer than ~280 K global mean temperature. For colder temperatures, the snow and ice albedo feedback becomes the dominant driver of the climate system. Here our purpose is to study climate changes driven by CO_2 for temperate and warmer states, modulated by water vapor and cloud feedbacks.

3. Equilibrium Climate Sensitivity Through Time

We first consider the case of repeated CO_2 doublings under the present-day solar insolation (1.0 S_0 = 1360 W/m^2; Figure 1a, black line). Conducting simulations at intervals of strict CO_2 doublings allows us to use ECS as a convenient metric for climate change (Figure 1b). Note that in this work we refer to CO_2 amounts in terms of partial pressure rather than volume mixing ratio. For low CO_2 amounts, the partial pressure in μbar (10^{-6} bar) approximately equals the volume mixing ratio in ppm relative to dry air (i.e., $pCO_2/(pN_2 + pCO_2)$); however, this approximation breaks down for $pCO_2 \gtrsim 0.1$ bar, because the total atmospheric pressure begins to grow larger than ~1 bar. We simulate modern Earth conditions with 1 bar N_2 and 360 μbar of CO_2, yielding a global mean surface air temperature of T_s = 288.7 K. This simulation is marked with a star on Figure 1a. Temperate climates (i.e., qualitatively similar to the modern Earth) can be maintained with CO_2 reduced down to at least 45 μbar, yielding T_s = 282.3 K.

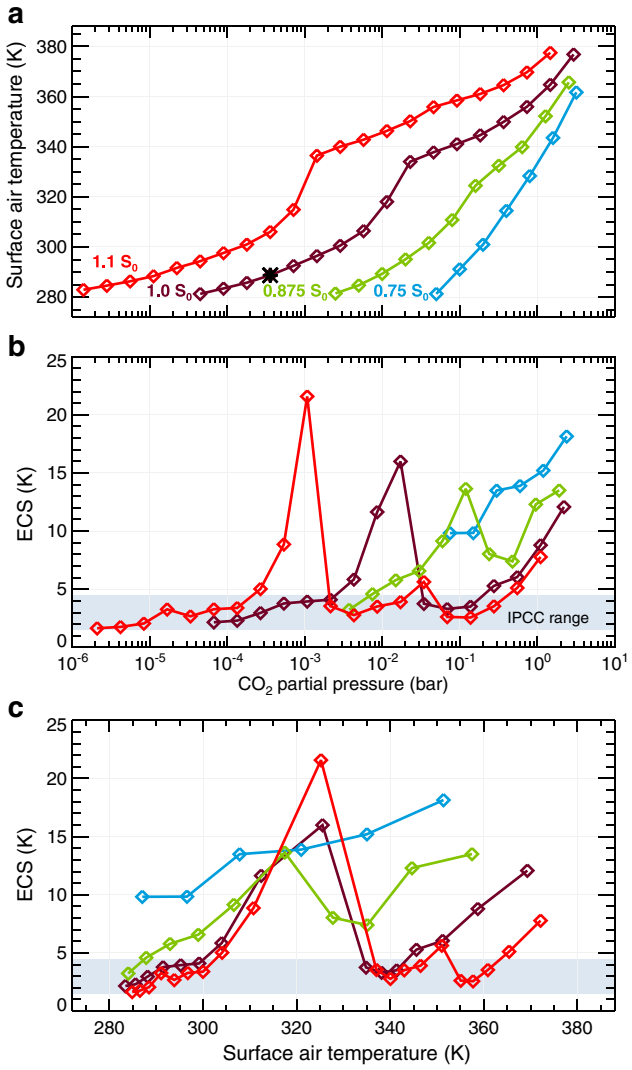

Figure 1. (a) Global mean surface air temperature and (b) equilibrium climate sensitivity (ECS) as a function of CO_2 partial pressure and under several values for the total solar insolation. (c) Equilibrium climate sensitivity (ECS) as a function of global mean surface air temperature. The temperatures shown in (c) are an average between the base and doubled-CO_2 state. The shaded region in (b) and (c) indicates the IPCC estimated range for ECS. Our nominal present-day Earth simulation is marked by an asterisk in (a), having a CO_2 partial pressure of 3.6×10^{-4} bar (equal to 360 μbar).

ECS for the first three CO_2 doublings beyond the present-day Earth (up to 2880 μbar CO_2) fall within the IPCC estimated range, with values of 3.8, 4.0, and 4.1 K, respectively (gray box in Figure 1b). At the fourth CO_2 doubling (5760 μbar CO_2), ECS exceeds the IPCC estimated range, reaching 5.8 K. Thus, the sensitivity of climate accelerates under potential anthropogenic CO_2 increases, in agreement with recent studies (Caballero & Huber, 2013; Meraner et al., 2013; Russell et al., 2013). We find a sharp maximum in ECS of 16.0 K evident at the sixth CO_2 doubling (0.02304 bar CO_2) beyond present-day Earth conditions. The maximum in ECS separates temperate climate states from a hot and water-rich climate state, often referred to as a "moist greenhouse." The term moist greenhouse was first used by Towe (1981) in reference to hot water-rich atmospheres speculated for the Hadean Earth. Both temperate and moist greenhouse states have similar values for ECS before and after the abrupt climate transition. Studies of solar-driven changes to Earth climate have found similar qualitative behavior in the climate sensitivity in response to strong solar (Leconte et al., 2013; Wolf & Toon, 2015) and also CO_2 forcings (Popp et al., 2016).

Next we consider CO_2 doublings applied to Earth at different points throughout its history and future; 0.75 S_0 (1020 W/m^2) corresponding to the early Archean ~3.8 Ga, 0.875 S_0 (1190 W/m^2) corresponding to the mid-Proterzoic ~1.9 Ga, and 1.1 S_0 (1496 W/m^2) corresponding to ~1 billion years into Earth's future. We find different climate responses to CO_2 doublings under each different solar constant. We find that the peak in ECS corresponding to the temperate to moist greenhouse transition increases in magnitude in proportion to the total solar insolation (Figure 1b). For 1.1 S_0, ECS behaves in a qualitatively similar fashion as does the present-day Earth case (1.0 S_0), but it has a more pronounced climate state transition, with a maximum value in ECS of 21.6 K and a value of ECS immediately before and after transition of <5 K. For 0.875 S_0, the climate transition becomes muted, attaining a maximum ECS of only 13.6 K, with values of ~6–8 K immediately before and after the transition. Finally, for 0.75 S_0, the temperate to moist greenhouse climate transition is not discernable via temperature and ECS indicators alone (Figures 1a and 1b). Instead, climate smoothly transitions between states, with ECS remaining large ($>$9.8 K) for all simulations conducted with 0.75 S_0.

It is helpful to recast ECS as a function of mean surface air temperature (Figure 1c). Note that the temperatures shown in Figure 1c are an average between the base and doubled-CO_2 state. The mean temperature of the planet dictates sea ice and atmospheric water vapor to first order, and thus imposes strong controls upon subsequent climatic feedbacks. By plotting ECS against temperature, we can normalize our results against temperature-dependent differences in the strength of these climate feedbacks. Note from Figure 1a that different CO_2 burdens are required to produce equal mean temperatures for a given value of the solar insolation. For both temperate climates ($T_s \leq 310$ K) and moist greenhouse climates ($T_s \geq 330$ K) considered separately, ECS increases with decreasing solar insolation. Thus, in these regimes, the early Earth under the faint Sun would have been significantly more sensitive to a doubling (or halving) of CO_2 than is the present-day Earth. For instance, given T_s~290 K as the initial temperature, a change in CO_2 by a factor of 2 results in an ~9.8 K change in T_s under 0.75 S_0, but only an ~3.8 K change under 1.0 S_0. An identical trend, but with greater differences, is seen for moist greenhouse climates. However, the behavior of climate under each solar insolation varies nonlinearly within the transition region (310 K $\geq T_s \geq$ 330 K). The sharp transition between temperate and moist greenhouse states becomes less pronounced under fainter solar insolation. For 0.75 S_0, ECS smoothly increases with temperature throughout this transition region. Note that the 1.1 S_0 curve appears to have additional small secondary peak in ECS centered

at T_s ~350 K that is absent from the other cases. Finally, also note that increases in ECS as function of mean surface temperature for temperate climates is in agreement with estimates based on paleoclimate reconstructions, spanning climate regimes from the Last Glacial Maximum with T_s ~283 K, to the Paleocene-Eocene thermal maximum with T_s ~303 K (Shaffer et al., 2016).

4. Forcing and Feedback Analysis

ECS is a valuable and easily understood metric for measuring climate change from CO_2. However, ECS conflates radiative forcings and climate feedbacks into a single quantity. Caballero and Huber (2013) suggested that variations in ECS may be attributed both to changes in the efficacy of CO_2 radiative forcings, as well as changes in climate feedbacks. Here we evaluate our simulations following the commonly used methods of Gregory et al. (2004) for analyzing radiative forcings and climate feedback within 3-D climate model simulations. The primary advantage of the Gregory et al. (2004) method is that it can easily be applied to standard monthly mean time series 3-D model outputs. No additional off-line or specially constructed radiative forcing calculations are required. A simple linear relationship is assumed between the net top-of-atmosphere energy imbalance, N (W/m^2), and the relative change in the mean surface air temperature, ΔT_s (K), given by $N = F - \alpha \Delta T_s$. F is the adjusted radiative forcing and α is the climate feedback parameter (W m^{-2} K^{-1}). When plotting N versus ΔT for the time series output of a simulation, F is then the y intercept and α is the slope of the line found through a linear regression. The climate feedback parameter, α, gives the radiative forcing required to change T_s by 1 K, and thus can generically be thought of as describing the inertia of climate system against radiative perturbations. Hansen et al. (2005) define the adjusted forcing as the radiative forcing present after allowing the stratospheric to adjust to a new thermal equilibrium; however, when following the Gregory et al. (2004) method, F also includes rapid adjustments that modify top-of-atmosphere fluxes on time scales of months, such as ultrafast cloud adjustments (Andrews et al., 2012).

In Figure 2, we plot the five-year running mean of N versus ΔT_s calculated at each model month, for all of our simulations conducted. N and ΔT_s are normalized against the coldest simulation conducted for each solar insolation, shown in Figure 1. Thus, $\Delta T_s = 0$ K corresponds to ~280 K for each case. Plotted in this fashion, the adjusted radiative forcing and the transient evolution of the climate system are elucidated for each subsequent CO_2 doubling. Note that it is necessary to use multiyear or even decadal mean values when using the Gregory et al. (2004) method in order to remove noise from internal variability of the climate system on shorter time scales.

As previously noted, a linear regression is typically used to determine F; however, such a method is not appropriate here because the time evolution of N with ΔT_s is nonlinear for cases with large implied radiative forcings and large integrated mean temperature changes. In Figure 3a we show the global mean clear-sky instantaneous outgoing longwave radiation, and in Figure 3b we show the associated change in outgoing longwave radiative forcing for subsequent CO_2 doublings from 1.4 μbar to 2.95 bar. While the adjusted radiative forcings takes into account changes in the stratosphere and ultrafast changes in clouds, humidity, and land/surface feedback (Gregory & Webb, 2008), the clear-sky instantaneous radiative forcing is a pure measure of changes to the CO_2 greenhouse effect. Here instantaneous forcings were calculated by outputting the radiative transfer calculations from the first time step, from each simulation, all of which share common initial conditions of the modern Earth on 1 January. Our findings support the idea that the radiative forcing imposed from CO_2 doublings increases with rising amounts of CO_2, however only up to about ~1.5-bar partial pressures. For the highest amounts of CO_2 used in this study (~3 bars), the increase in the adjusted radiative forcings slows. Here while doubling CO_2 from the present-day conditions produces an adjusted forcing of only $\Delta F = 3.9$ W/m^2, increasing CO_2 from 0.1 to 0.2 bars yields $\Delta F = 11$ W/m^2. Our results are in agreement with Halevy et al. (2009), who showed with line-by-line calculations that CO_2 doublings for early Earth and early Mars-like atmospheres, with $pCO_2 > 0.1$ bar, result in reductions to the outgoing longwave radiation of 10–20 W/m^2, and with a similar trend with increasing pCO_2 as found here. For Earth under the faint young Sun, large amounts of CO_2 are required to sustain temperate climates. For the early Archean and mid-Proterozoic, 0.05 and 0.0025 bar of CO_2 are required to maintain T_s ~282 K, respectively (Figure 1). Subsequent CO_2 doublings are accompanied by stronger imposed radiative forcings, which contribute to producing larger changes in temperature for each doubling. On the other hand for 1.1 S_0, only 1.4 μbar of

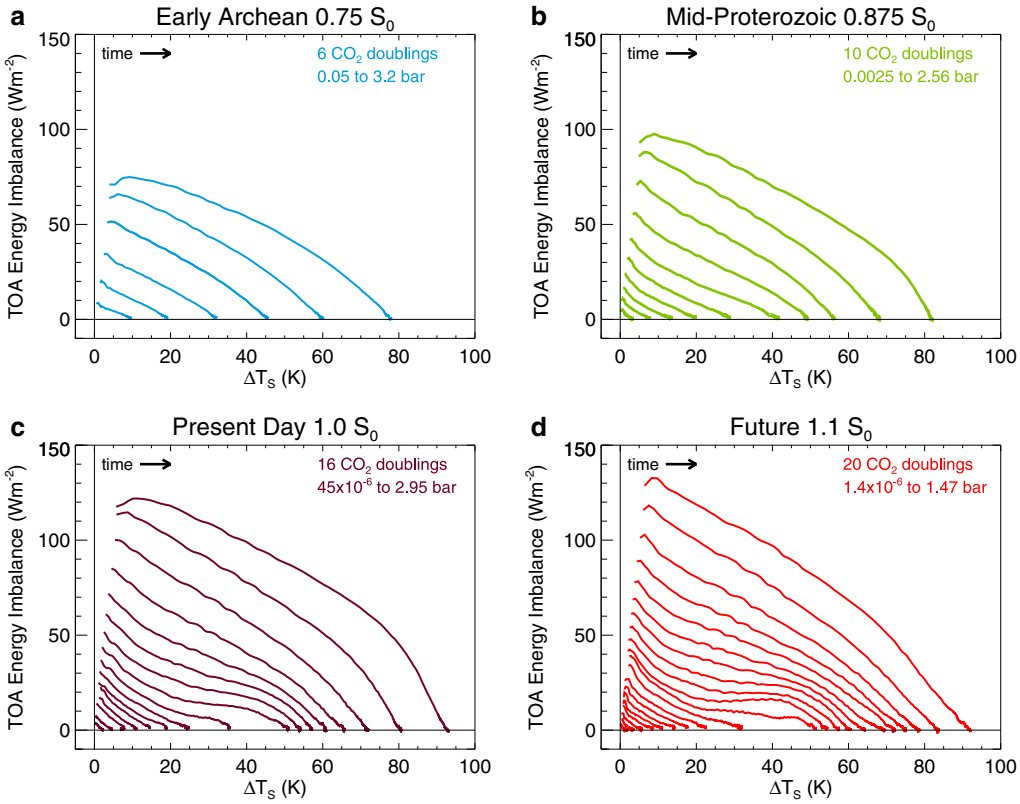

Figure 2. Gregory et al. (2004) analysis plots of all simulations, under (a) 0.75 S_0, (b) 0.875 S_0, (c) 1.0 S_0, and (d) 1.1 S_0. We plot the running five-year mean top-of-atmosphere energy imbalance (N) versus temperature change (ΔT_s) of the time series for each simulation. N and ΔT are normalized to the coldest simulations conducted under each insolation. The arrow indicates the flow of time. Note that $\Delta T_s = 0$ K corresponds to ~280 K for each case.

CO_2 is needed to maintain a temperate climate, and numerous subsequent CO_2 doublings impose only a small adjusted radiative forcing.

However, the magnitudes of the radiative forcings do not tell the whole story. The assumed linear relation between N and ΔT_s breaks down for large forcings and their resultant changes in temperature. The nonlinear evolution of surface temperature is caused by climate feedbacks that respond to the implied radiative forcing. The strength of the climate feedback is independent of the implied initial radiative forcing and is thus a measure of the change in temperature caused by adjustments to the climate system as new equilibrium conditions are reached. Bloch-Johnson et al. (2015) argued that the linear approximation between N and ΔT_s should be amended with higher-order terms that allow for a better representation of temperature-dependent climate feedbacks. Here for small warming ($\Delta T_s < 20$ K), a linear relationship between N and ΔT_s remains generally valid. For cases of extreme warming ($\Delta T_s > 60$ K), the resultant temperatures at equilibrium are less than if a strictly linear response had occurred. Bloch-Johnson et al. (2015) suggest that such behavior is caused by a (negative) quadratic temperature-dependent feedback. Most curiously, here intermediary warmings ($20 \leq \Delta T_s \leq 60$ K), particularly for 1.0 S_0 and 1.1 S_0 cases, display a complex evolution between N and ΔT_s which may be best modeled with the addition of either cubic or quintic temperature-dependent climate feedback terms (e.g., Bloch-Johnson et al., 2015, Figures S1 and S2).

For the case of nonlinear climate feedback, Gregory et al. (2004) suggest computing the "differential climate parameter" by taking the derivative of the curves shown in Figure 2, where $\alpha_{diff} = -dN/d\Delta T_s$, and thus, α_{diff} is the instantaneous slope of the line tangent to the curves shown in Figure 2. In Figure 4, we plot α_{diff} computed for all simulations, based on the five-year running averages of N and ΔT_s that are shown in Figure 2. However, even when using five-year running averages, internal variability of the climate system (i.e., seasons, weather) causes considerable scatter in α_{diff}. As a steady state is reached ($N \rightarrow 0$), the denominator in the

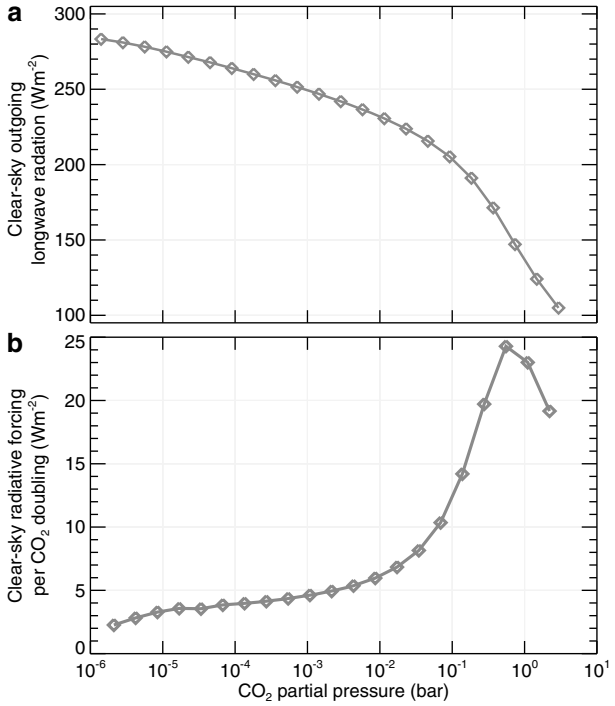

Figure 3. (a) Global mean instantaneous clear-sky outgoing longwave radiation and (b) the radiative forcings for each CO_2 doubling, respectively.

above equation ($d\Delta T_s$) becomes small while the energy imbalance (N) oscillates around zero due to internal variability. This results in large and oscillating values of α_{diff} after equilibrium is reached that are not representative of the decadal-scale climate responses to implied CO_2 radiative forcings. We exclude these points (gray points in Figure 4) from our fitting procedure for α_{diff}. We then construct least squares polynomial fits of $\alpha_{diff}(\Delta T)$ using the mean values of α_{diff} binned at each temperature.

We find that α_{diff} changes as a function of temperature and is different for each solar constant. Note that larger values of α_{diff} imply a muted climate feedback, while small values of α_{diff} imply a strong positive climate feedback. The simulations under mid-Proterzoic, present-day, and future Earth solar constants display qualitatively similar behavior, where α_{diff} decreases between $0 \leq \Delta T_s \leq 35$ K, before increasing at higher temperatures. The decrease in α_{diff} as $\Delta T_s \rightarrow 35$ K describes the sharp climate transition shown in Figure 1. Curiously, α_{diff} remains linear and increasing for all temperatures for the early Archean cases. In all cases, for large ΔT_s the climate becomes more resistant to change.

The climate feedback parameter (W m^{-2} K^{-1}) is the inverse of specific climate sensitivity (K (W/m^2)$^{-1}$). Specific climate sensitivity, $1/\alpha$, represents the temperature change caused by imposing a 1 W/m^2 radiative forcing, and may be more intuitive to consider compared to the climate feedback parameter. In Figure 5a we plot specific climate sensitivity versus the mean surface air temperature, using the inverse of the polynomial fits of α_{diff} found in Figure 4. Constructed in this fashion, Figure 5a illustrates the time-evolving behavior of climate sensitivity as the climate warms. Cases at 1.1, 1.0, and 0.875 S_0 display a peak in climate sensitivity centered near 315 K, with the magnitude of the peak inversely dependent on the solar insolation. The early Archean case (0.75 S_0) exhibits linearly decreasing climate sensitivity with increasing surface temperature. For all cases, we do not see an increase in climate sensitivity at high surface temperatures (>340 K), like what is found for ECS in Figure 1c. Enhanced ECS for the paleoclimates and generally at high surface temperature is caused by an increase in the strength of radiative forcing from CO_2 at high partial pressures rather than from climate feedbacks, which become muted. Of concern for the present-day Earth, both the climate sensitivity and ECS increase for $280 \leq T_s \leq 315$ K. Thus, warming due to anthropogenic CO_2 emissions may be aggravated by nonlinear climate feedbacks. In Figure 5b we plot the climate sensitivity calculated as $\Delta T_s/F$, where F is taken as the instantaneous radiative forcing per CO_2 doubling shown in Figure 3b. Constructed in this fashion, Figure 5b illustrates the time-integrated climate sensitivity, thus after climate has fully adjusted and a new equilibrium has been reached. The time-integrated and time-evolving sensitivities exhibit qualitatively similar behavior, with a discernable peak in sensitivity occurring for high-insolation cases (1.0 and 1.1 S_0) centered at ~320 K.

5. Cloud Feedback

Climate feedback shown in Figures 4 and 5 isolate responses of the climate system from the effects of pure radiative forcings. Differences in the evolution of climate sensitivity as a function of surface temperature and solar insolation arise due to the interplay between radiative and cloud processes. These can be understood in terms of the evolution of the global mean albedo components as a function of the mean surface air temperature (Figure 6). The top-of-atmosphere albedo includes the contributions from clouds, air (i.e., Rayleigh scattering), and surface. Decreases to the surface albedo (Figure 6d) with increasing T_s are a direct consequence of shrinking sea ice and continental snow cover as the climate warms, with identical behavior under all values of the solar constant. Changes to the clear-sky albedo are due to a combination of the surface albedo and Rayleigh scattering, the latter of which increases for thick CO_2-dominated atmospheres. CO_2 is ~2.5 times more effective at scattering compared to N_2 (Kasting, 1991) and becomes significant for CO_2 partial pressures ≥0.1 bar (e.g., Figures 1a and 6c). Note that the hottest simulations conducted here have up to 3.2 bars of CO_2

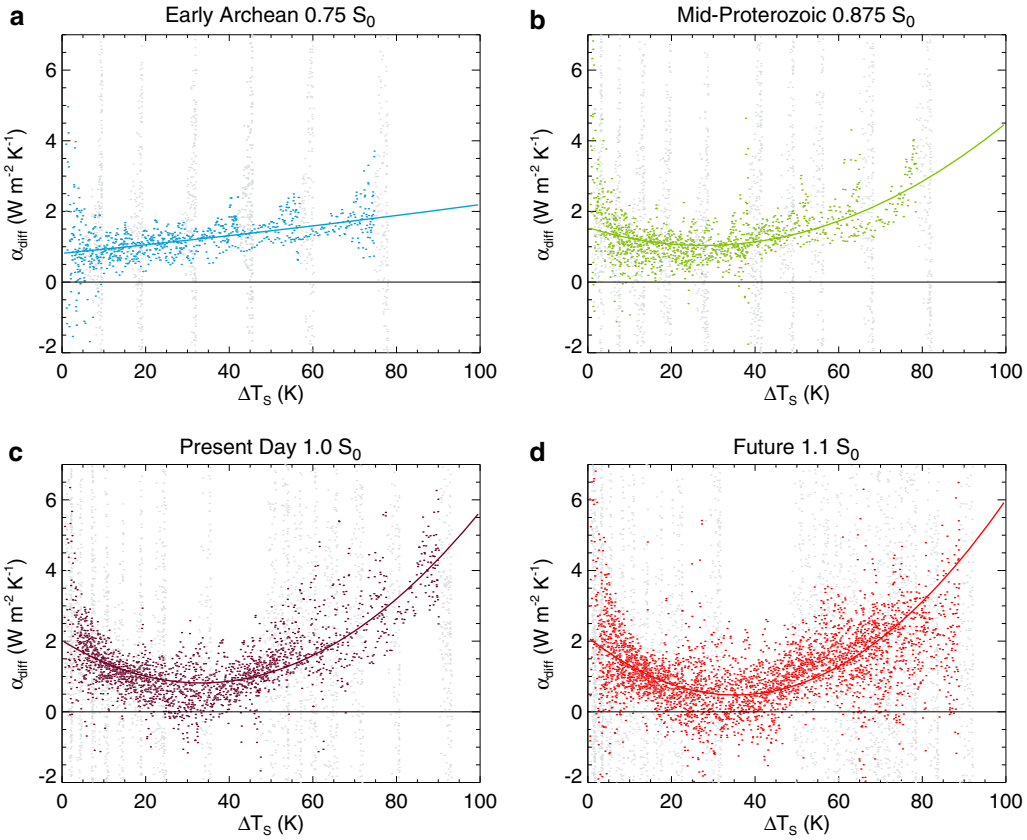

Figure 4. The differential climate feedback parameter (α_{diff}) versus change in temperature (ΔT). Gray points are omitted from analysis, as they represent the internal variability of the model in equilibrium (i.e., when $\overline{N} > 0$). The solid line shows a least squares polynomial fit for α_{diff} (ΔT). Larger values of α_{diff} imply muted climate feedback, while small values of α_{diff} imply strong positive climate feedback. Note that $\Delta T_s = 0$ K corresponds to ~280 K for each case.

(in addition to 1 bar N_2). Plotted as a function of T_s, Rayleigh scattering becomes progressively stronger for warm (>300 K) climates under weaker solar insolations because more CO_2 is required to reach these warm surface temperatures, resulting in a thick scattering atmosphere.

The cloud albedo exhibits a systematic dependence on the solar insolation (Figure 6b). Previous 3-D climate modeling of the Archean Earth resulted in fewer tropical clouds and subsequently reduced cloud albedos. This is a consequence of the faint young Sun. Less solar energy is incident on tropical oceans, reducing surface evaporation rates, latent heat fluxes, and ultimately low-level clouds (Wolf & Toon, 2013). Similarly, here we find that the global mean cloud albedo varies in proportion with the solar insolation at all values of T_s (Figure 6b), and across a range of insolations. Under all solar constants cloud feedbacks have a destabilizing effect on climate for $280 \leq T_s \leq 330$ K. That is, warming climate leads to reductions in the cloud albedo, thus constituting a positive climate feedback and leading to further warming. The sharp transition between temperate and moist greenhouse climate states centered at T_s ~320 K is associated with the minima in cloud albedo (Figure 6b), and is caused by the convective stabilization of warm atmospheres and subsequent dissipation of low-lying clouds as reported in Wolf and Toon (2015). For hotter temperatures ($340 \leq T_s \leq 380$ K), climates can remain stable against a runaway greenhouse due to an increase in the planetary albedo from the combined action of a rebound in the cloud albedos and increased Rayleigh scattering from denser CO_2 atmospheres required to attain such warming. Wolf and Toon (2015) attribute this increase in cloud albedo at hotter planetary temperatures to increased solar absorption by water vapor aloft, which drives convection emanating from the middle troposphere, thickening high-altitude clouds.

In Figure 7 we show global mean vertical profiles of the grid box-averaged cloud water (kg/m^3), as a function T_s for simulations under 0.75 S_0, 0.875 S_0, 1.0 S_0, and 1.1 S_0, respectively. Cloud condensate is a better

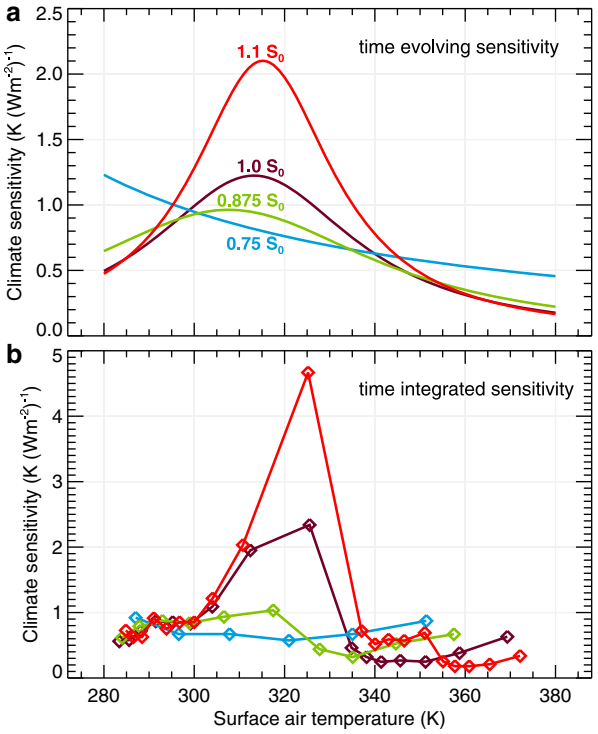

Figure 5. Specific climate sensitivity as a function of surface air temperature (a) determined from our polynomial fits for α_{diff} and (b) calculated from $\Delta T_s/F$, where ΔT_s is the total temperature change and F is the instantaneous forcing. Thus, (a) illustrates the time evolution of climate sensitivity as the planet warms, while (b) illustrates the time-integrated climate sensitivity, after new equilibrium states have been reached.

indicator of the cloud radiative effects in the model than is cloud fraction, as sometimes large cloud fractions can be diagnosed when relatively little cloud condensate is actually present. Note that while the cloud level moves upward in the atmosphere as the climate warms, the temperature of cloud formation remains largely unchanged between ~275 and ~225 K. Wolf and Toon (2015) previously argued that the sharp spike in climate sensitivity occurring between $310 \leq T_s \leq 330$ K (seen also here in Figure 1 here) is triggered by a radiative-convective-cloud feedback. Increasing the radiative opacity of the low atmosphere due to increasing water vapor in warm atmospheres causes increased absorption of solar energy in the near-infrared, which stabilizes the boundary layer against convection, reducing cloud water, the cloud albedo, and thus the planetary albedo, resulting in a spike in T_s. This process similarly occurs for CO_2-driven climate warming. In Figure 7 we have bracketed the temperature region associated with this climate transition with vertical dashed lines. As global mean temperatures rise from modern Earth-like values through the climate transition region, clouds located below ~5 km dissipate, resulting in the cloud albedo reductions (Figure 6b). Beyond 330 K, the upper atmospheric cloud deck begins to thicken and cloud albedos increase and stabilize climate (Figure 6b). Here we find that these modulations of the cloud water and cloud albedo are progressively stronger under higher solar insolations. Under higher solar constants, evaporation and ocean–atmosphere latent heat fluxes are proportionally stronger, resulting in more clouds and larger cloud albedos in the initial state (i.e., modern-Earth-like T_s). Conversely, under weak solar insolation there are fewer clouds, and a lower cloud albedo to begin with (Figures 6b and 7) and subsequent modulations to clouds and the climate transition are muted. Thus, under weak solar radiation, a stabilization of the boundary layer at the moist greenhouse transition has a more limited impact on the clouds, albedo, and thus the climate.

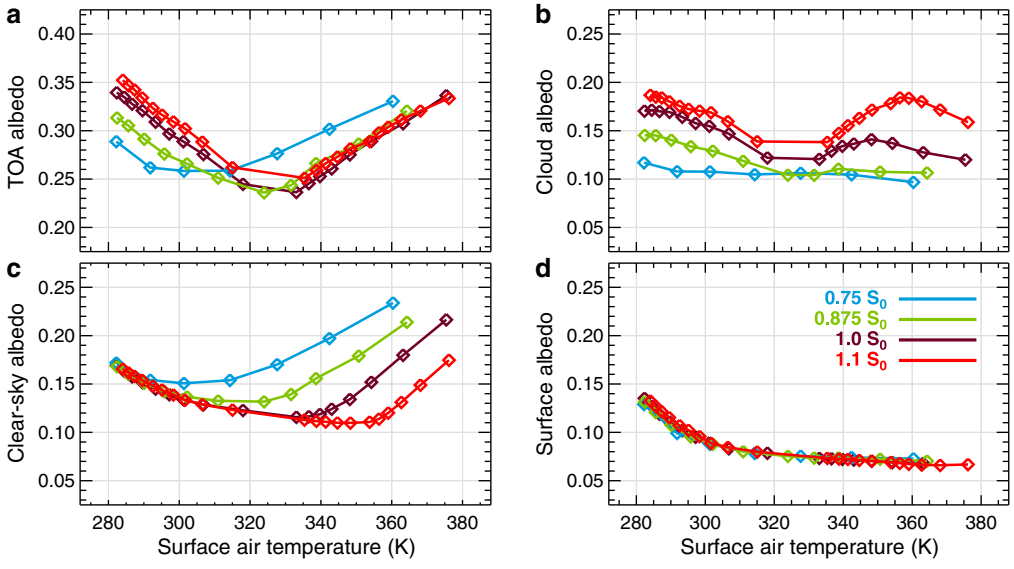

Figure 6. (a) Global mean top-of-atmosphere albedo, (b) cloud albedo, (c) Rayleigh scattering albedo, and (d) surface albedo as a function of global mean surface air temperature and under several values of the total solar insolation.

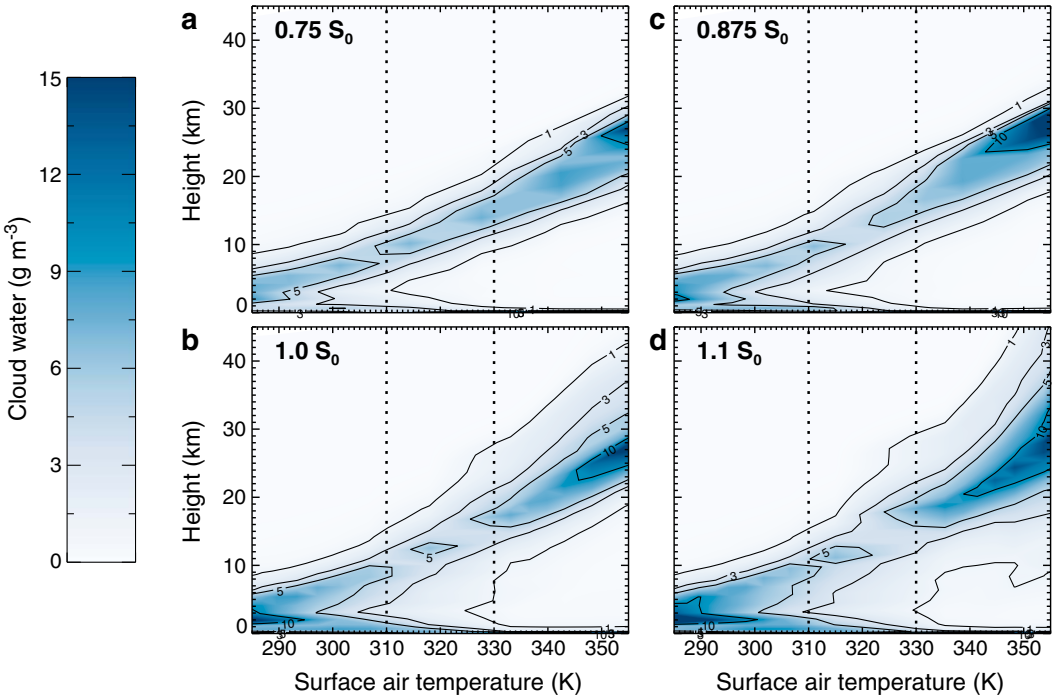

Figure 7. Global mean vertical profiles of the grid box averaged cloud water as a function of mean surface temperature for 0.75 S_0, 0.875 S_0, 1.0 S_0, and 1.1 S_0 simulation sets, respectively. The vertical dashed lines highlight the temperature region where an abrupt change in climate occurs for higher solar constants.

Finally, Caballero and Huber (2010, 2013) have argued that equatorial superrotation in the upper troposphere emerges for warming climates when tropical sea surface temperatures exceed ~306 K. They credit the development of superrotating winds for creating strong vertical wind shear, which in turn affects convective organization and limits the formation of middle- and high-level clouds in the tropics, thus reducing planetary albedos. Here we similarly find a transition to superrotation with warming climates, albeit corresponding with the moist greenhouse transition in model at T_s ~320 K (Figure 8). Thus, while we have generally explained the breakup of clouds and subsequent reduction in cloud albedos in a radiative-convective sense (e.g., Wolf & Toon, 2015), atmospheric dynamical processes may also be contributing to the modulation of clouds seen in this set of simulations. In future work, we hope to examine the robustness of the occurrence of superrotation and its influence on clouds for warming climates, across different models and under different atmospheric assumptions. In this section we have focused on the role of shortwave feedbacks in modulating climate sensitivity. Future work may also examine the effects of other feedbacks, such as lapse rate, water vapor greenhouse, and cloud longwave, using more advanced techniques such as the partial radiative perturbation (Colman & McAvaney, 1997) and radiative kernel (Soden et al., 2008) methods. However, these methods require the climate model to be run in different modes of operation and with different data outputs that were not used here.

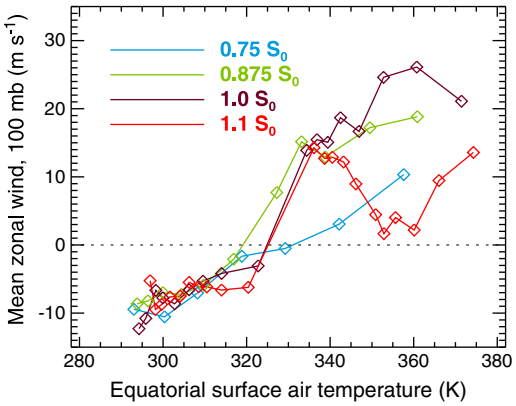

Figure 8. Zonal mean equatorial wind speeds at 100-mb pressures, plotted against equatorial mean surface temperatures. The moist greenhouse transition, centered at ~320 K, is accompanied by a transition to superrotation in the upper troposphere.

6. Discussions

Our results have important ramifications for past, present, and future climates of Earth. Given approximately modern Earth-like temperatures, large equilibrium climate sensitivities under reduced solar constants (e.g., 0.75 S_0 and 0.875 S_0) imply that the climate of paleo-Earth was intrinsically less stable against changing atmospheric CO_2 burdens. Thus, warming the early Earth despite the faint young Sun may have benefited from

this enhanced climate sensitivity to doubling CO_2. Fewer doublings of CO_2 (above the present level) are needed to maintain a temperate climate. This is partially due to the increased efficacy of CO_2 radiative forcings for the high amounts expected at early times in Earth history, and also partially due to changes in the shortwave cloud feedback as discussed in section 5. However, enhanced climate sensitivity works in both directions, allowing potentially more drastic cooling periods if CO_2 is drawn down when weathering rates outpace volcanic outgassing. Thus, climate movements into and out of glacial (but nonsnowball) periods may have occurred more readily on Earth in the distant past.

Based on our results, it appears unlikely that extreme warmth predicted for the Archean Earth from oxygen and silicone isotopes in ancient cherts (Knauth & Lowe, 2003; Robert & Chaussidon, 2006) can be reached with CO_2 alone. In addition to our 1-bar N_2 background, 0.8 bar CO_2 is needed to attain T_s = 328 K at 3.8 Ga (0.75 S_0), and 0.32 bar CO_2 is needed to attain T_s = 332 K at 1.9 Ga (0.875 S_0). However, these large values for CO_2 may be implausibly large. For instance, Driese et al. (2011) constrain paleo-CO_2 to only ~0.02 bar circa 2.69 Ga. Sheldon (2006) constrains CO_2 at 2.5 Ga to be at most about 0.03 bar with a most probable value of less than ~0.01 bar. If similar amounts of CO_2 remained present in the atmosphere at 1.9 Ga, global surface mean temperatures would only be between 290 and 300 K. Furthermore, other lines of geochemical evidence constrain the total pressure of the atmosphere to be equal to or possibly below modern levels (Marty et al., 2013; Som et al., 2012), implying that multibar early atmospheres unlikely.

To more immediate concerns, humans face the threat of warming climate due to anthropogenic climate change. In section 3 we studied cases relevant to anthropogenic warming, with the modern Earth subjected to numerous doublings of CO_2. Fortunately, humans could not feasibly drive the Earth into a runaway greenhouse, with even multibar CO_2 atmospheres being insufficient to do so. This result is in agreement with the original 1-D radiative-convective modeling of Kasting and Ackerman (1986). More recent 1-D modeling work found that the Earth may runaway under only 12 times the preindustrial value for CO_2; however, the authors argue that more complete treatments of clouds and relative humidity would likely make Earth climate significantly more stable against a runaway for high values of CO_2 (Ramirez et al., 2014). Extreme anthropogenic changes to CO_2, where large amounts of fossil fuels are burned rapidly, may *only* yield several thousand ppm of CO_2 (Ramirez et al., 2014). In our model, ~2880 ppm of CO_2 yields global mean surface air temperatures of only 300.6 K. Still, while such a climate state falls several CO_2 doublings short of the moist greenhouse transition (e.g., Figure 1a) and well short of the "Venus syndrome" described by Hansen (2010), such an Earth would doom much of human population to prolonged periods of lethal heat stress (Sherwood & Huber, 2010).

With the modern greenhouse gas concentration, at 1.1 S_0 (equivalent to about 1 billion years in the future), the mean surface temperature of Earth will be ~307 K. Disconcertingly, the transition to a moist greenhouse state occurs when $pCO_2 = 1440 \times 10^{-6}$ bar, only two CO_2 doublings in our model. However, advanced human civilization may stand a chance for the successful long-term regulation of planetary climate. If atmospheric CO_2 could be drawn down, or if incident solar radiation could be reflected away, then moderate temperatures could be maintained despite the brightening Sun. Despite a 10% increase in solar insolation, if CO_2 were drawn down to 11.25×10^{-6} bar (~3% of the modern level), then T_s = 288.3 K. Such drastic regulation of CO_2 may eventually become necessary to preserve human habitability on the planet. Of course, limiting CO_2 to such a degree would threaten plant biology and present new and unforeseen challenges to the living Earth as we know it. Another climate management option involving solar radiation management would deploy a planetary-scale reflector to reduce incident solar radiation. Such options for geoengineering the climate system are being discussed for responding to climate change today, but geoengineering could also help maintain habitable conditions on Earth in the distant future (Goldblatt & Watson, 2012).

Finally, we remind the reader that these results come from only a single climate model. While adjusted forcing from CO_2 should be robust across models (e.g., Halevy et al., 2009), feedbacks involving clouds are uncertain, and may be model and resolution dependent. Temperature responses of 3-D models even to a single CO_2 doubling beyond the present day may vary by ~2 K (Rogelj et al., 2012). Differences may become greater when attempting to model more extreme conditions. For instance, Popp et al. (2016) using an idealized version of the ECHAM model, found that Earth may transition to a moist greenhouse state under only four CO_2 doublings. However, they note that idealizations in their model (i.e., ice-free, aquaplanet, zero obliquity) result

in warmer temperatures for control simulations, and greater climate sensitivities than Earth-configured versions of the same model (e.g., Meraner et al., 2013). Furthermore, the core model we have used was designed originally to deal with Earth. Although we have taken care to ensure that the atmospheric compositions are self-consistently modeled, and CAM does take into account changes in pressure and thermodynamics of water vapor (Neale et al., 2010), the cloud, convection, and boundary layer routines still may be pushed beyond their design parameters. Encouragingly, climate modeling studies with different models (e.g., Meraner et al., 2013; Popp et al., 2016; Russell et al., 2013) indicate qualitative similarities in their model responses of present-day Earth to large CO_2 forcings.

7. Conclusions

The combined variations of the solar insolation and atmospheric CO_2 impart primary controls on the evolution of Earth's global mean temperature over the course of its history. The work presented here demonstrates that the sensitivity of climate to changing CO_2 is dependent upon both the absolute CO_2 concentration, and upon climate feedbacks that are dependent on the global mean surface temperature. Note that the global mean temperature implicitly dictates the partitioning of water among its thermodynamic phases within the climate system, which in turn influences the strength of climate feedbacks involving clouds, water vapor, and sea ice. In agreement with previous studies, we find that the adjusted radiative forcing from doubling CO_2 increases at high concentrations. Thus, when phrased in terms of equilibrium climate sensitivity, paleoclimates (under weak solar insolation but with implicitly larger CO_2 inventories) experience relatively larger (~10 W/m^2) changes in the adjusted radiative forcings for each CO_2 doubling. This change in forcing generally results in correspondingly larger changes in temperature compared with estimates of ECS made for anthropogenic climate change studies.

However, ECS and radiative forcing do not tell the whole story. Climate feedbacks are responsible for amplifying (or muting) imposed radiative forcings. The combination of radiative forcings and climate feedbacks yields the total change in temperature expected. A strong nonlinear feedback in the climate system is identified as a sharp climatic transition between a temperate climate state ($T_s < 310$ K) and a hot and moist state ($T_s > 330$ K). This abrupt climatic transition is associated with temperature-dependent cloud albedo feedback, which are independent of the implied radiative forcing. We also find that the cloud albedo feedback behaves differently depending upon the solar constant relevant to each time period of interest in Earth's history. Under weak solar insolation, cloud albedos are low, there is very little modulation of the clouds with changing mean surface temperatures, and the change in temperature with increasing CO_2 remains approximately linear. Under strong solar insolation, cloud albedos experience a significantly greater degree of modulation, and thus act as a strong nonlinear feedback upon the climate system. It is evident that climate sensitivity to changing CO_2 varies if the strength of the solar constant, the CO_2 partial pressure, or the mean temperature of the planet is significantly different.

Acknowledgments
E.T. Wolf thanks NASA Planetary Atmospheres Program award NNH13ZDA001N and NASA Astrobiology Institute CAN7 award NNH13DA017C through participation in the Nexus for Exoplanet System Science. J. Haqq-Misra thanks support from the Virtual Planetary Laboratory under award NNA13AA93A. O.B. Toon thanks NASA Habitable Worlds Award NNX16A080G. This work utilized the Janus supercomputer, which was supported by the National Science Foundation (award CNS-0821794) and the University of Colorado at Boulder. We thank D. Abbot for the helpful discussions. The core model used in this study, CESM1.2, is freely available to all at http://www.cesm.ucar.edu/models/cesm1.2/via the National Center for Atmospheric Research, Boulder, CO. The specific code changes we have made to the model, along with necessary initial files and directions for implementation into CESM, are available on Github via the following code packages; https://github.com/storyofthewolf/ExoRT contains the radiative transfer code used and https://github.com/storyofthewolf/ExoCAM contains CESM configurations and minor code changes. The model outputs used in this study, including multiyear mean climates at equilibrium and time series climate statistics used for forcing-feedback analysis, have been made publicly available at the The Internet Archive (https://archive.org/details/EvaluatingClimateSensitivityToCO2AcrossEarthsHistory_201809). No competing financial interests exist.

References

Andrews, T., Gregory, J. M., Wenn, M. J., & Taylor, K. E. (2012). Forcing, feedbacks, and climate sensitivity in CMIP5 coupled atmosphere-ocean climate models. *Geophysical Research Letters*, *39*, L709712. https://doi.org/10.1029/2012GL051607

Bitz, C. M., Shell, K. M., Gent, P. R., Bailey, D. A., & Danabasoglu, G. (2012). Climate sensitivity of the Community Climate System Model, version 4. *Journal of Climate*, *25*(9), 3053–3070. https://doi.org/10.1175/JCLI-D-11-00290.1

Blake, R. E., Chang, S. J., & Lepland, A. (2010). Phosphate oxygen isotopic evidence for a temperate and biologically active Archaean Ocean. *Nature*, *464*(7291), 1029–1032. https://doi.org/10.1038/nature08952

Bloch-Johnson, J., Pierrehumbert, R. T., & Abbot, D. (2015). Feedback temperature dependence determines the risk of high warming. *Geophysical Research Letters*, *42*, 4973–4980. https://doi.org/10.10002/2015GL064240

Budyko, M. I. (1969). The effect of solar radiation variations on the climate of the Earth. *Tellus*, *21*, 611–619.

Caballero, R., & Huber, M. (2010). Spontaneous transition to superrotation in warm climates simulated by CAM3. *Geophysical Research Letters*, *37*, L11701. https://doi.org/10.1029/2010GL043468

Caballero, R., & Huber, M. (2013). State-dependent climate sensitivity in past warm climates and its implications for future climate predictions. *Proceedings of the National Academy of Sciences of the United States of America*, *110*(35), 14,162–14,167. https://doi.org/10.1073/pnas.1303365110

Charnay, B., Forget, F., Wordsworth, R., Leconte, J., Millour, E., Codron, F., & Spiga, A. (2013). Exploring the faint young Sun problem and the possible climates of the Archean with a 3-D GCM. *Journal of Geophysical Research: Atmospheres*, *118*, 10,414–10,431. https://doi.org/10.1002/jgrd.50808

Charney, J. (1979). *Carbon Dioxide and Climate: A Scientific Assessment* (p. 33). Washington, DC: National Academy of Sciences Press.

Clough, S. A., Shephard, M. W., Mlawer, E. J., Delamere, J. S., Iacono, M. J., Cady-Pereira, K., et al. (2005). Atmospheric radiative transfer modeling: A summary of the AER codes. *Journal of Quantitative Spectroscopy and Radiative Transfer*, *91*(2), 233–244.

Colman, R. A., & McAvaney, B. J. (1997). A study of general circulation model climate feedbacks determined from perturbed sea surface experiments. *Journal of Geophysical Research*, *102*(D16), 19,383–19,402. https://doi.org/10.1029/97JD00206

Danabasoglu, G., & Gent, P. R. (2009). Equilibrium climate sensitivity: Is it accurate to use a slab ocean model? *Journal of Climate*, *22*, 2494. https://doi.org/10.1175/2008JCLI2596.1

Donnadieu, Y., Ramstein, G., Fluteau, F., Roche, D., & Ganopolsku, A. (2004). The impact of atmospheric and oceanic heat transports on the sea-ice-albedo instability during the Neoproterozoic. *Climate Dynamics*, *22*, 293–306.

Driese, S. G., Jirsa, M. A., Ren, M., Brantley, S. L., Sheldon, N. D., Parker, D., & Schmitz, M. (2011). Neoarchean paleoweathering of tonalite and metabasalt: Implications for reconstructions of 2.69 Ga early terrestrial ecosystems and paleoatmospheric chemistry. *Precambrian Research*, *189*(1-2), 1–17. https://doi.org/10.1016/j.precamres.2011.04.003

Forster, P. M., Andrews, T., Good, P., Gregory, J. M., Jackson, L. S., & Zelinka, M. (2013). Evaluating adjusted forcing and model spread for historical and future scenarios in the CMIP5 generation of climate models. *Journal of Geophysical Research: Atmospheres*, *118*, 1139–1150. https://doi.org/10.1002/jgrd.50174

Goldblatt, C., Claire, M. W., Lenton, T. M., Matthews, A. J., Watson, A. J., & Zahnle, K. J. (2009). Nitrogen-enhances greenhouse warming on early Earth. *Nature Geoscience*, *2*(12), 891–896. https://doi.org/10.1038/ngeo692

Goldblatt, C., & Watson, A. J. (2012). The runaway greenhouse: implications for future climate change, geoengineering and planetary atmospheres. *Philosophical Transactions of the Royal Society A*, *370*(1974), 4197–4216. https://doi.org/10.1098/rsta.2012.0004

Goldner, A., Herold, N., & Huber, M. (2014). The challenge of simulating the warmth of the mid-Miocene climate optimum in CESM1. *Climate of the Past*, *10*(2), 523–536. https://doi.org/10.5194/cp-10-523-2014

Goldner, A., Huber, M., & Caballero, R. (2013). Does Antarctic glaciation cool the world? *Climate of the Past*, *9*(1), 173–189. https://doi.org/10.5194/cp-9-173-2013

Gough, D. O. (1981). Solar interior structure and luminosity variations. *Solar Physics*, *74*(1), 21–34. https://doi.org/10.1007/BF00151270

Gregory, J., & Webb, M. (2008). Tropospheric adjustment induces a cloud component in CO_2 forcing. *Journal of Climate*, *21*(1), 58–71. https://doi.org/10.1175/2007JCLI1834.1

Gregory, J. M., Ingram, W. J., Palmer, M. A., Jones, G. S., Stott, P. A., Thorpe, R. B., et al. (2004). A new method for diagnosing radiative forcing and climate sensitivity. *Geophysical Research Letters*, *31*, L03205. https://doi.org/10.1029/2003GL018747

Halevy, I., Pierrehumbert, R. T., & Schrag, D. P. (2009). Radiative transfer in CO_2-rich paleoatmospheres. *Journal of Geophysical Research*, *114*, D18112. https://doi.org/10.1029/2009JD011915

Hansen, J., Sato, M., Ruedy, R., Nazarenko, L., Lacis, A., Schmidt, G. A., et al. (2005). Efficacy of climate forcings. *Journal of Geophysical Research*, *110*, D18104. https://doi.org/10.1029/2005JD005776

Hansen, J. E. (2010). *Storms of my Grandchildren*, *The Truth about the Coming Climate Catastrophe and our Last Chance to Save Humanity*. NY: Bloomsbury.

Haqq-Misra, J. D., Domagal-Goldman, S. D., Kasting, P. J., & Kasting, J. F. (2008). A revised, hazy methane greenhouse for the Archean Earth. *Astrobiology*, *8*(6), 1–11.

Hessler, A. M., Lowe, D. R., Jones, R. L., & Bird, D. K. (2004). A lower limit for atmospheric carbon dioxide levels 3.2 billion years ago. *Nature*, *428*(6984), 736–738. https://doi.org/10.1038/nature02471

Hoffman, P. F., Kaufman, A. J., Halverson, G. P., & Schrag, D. P. (1998). A Neoproterozoic snowball Earth. *Science*, *281*(5381), 1342–1346. https://doi.org/10.1126/science.281.5381.1342

Holland, H. D. (2006). The oxygenation of the atmosphere and oceans. *Philosophical Transactions of the Royal Society B*, *361*(1470), 903–915. https://doi.org/10.1098/rstb.2006.1838

Hren, M. T., Tice, M. M., & Chamberlain, C. P. (2009). Oxygen and hydrogen isotope evidence for a temperate climate at 3.42 billion years ago. *Nature*, *462*(7270), 205–208. https://doi.org/10.1038/nature08518

IPCC (1990). *Climate Change: The IPCC Scientific Assessment* (p. 365). Cambridge: Cambridge University Press.

IPCC (2014). In Core Writing Team, R. K. Pachauri, & L. A. Meyer (Eds.), *Climate Change 2014: Synthesis Report. Contribution of Working Groups I, II, and III to the Fifth Assessment Report of the Intergovernmental Panel on Climate Change* (p. 1151). Geneva, Switzerland: IPCC.

Kasting, J. F. (1987). Theoretical constraints on oxygen and carbon dioxide concentrations in the Precambrian atmospheres. *Precambrian Research*, *34*(3-4), 205–229. https://doi.org/10.1016/0301-9268(87)90001-5

Kasting, J. F. (1991). CO_2 condensation and the climate of early Mars. *Icarus*, *94*(1), 1–13. https://doi.org/10.1016/0019-1035(91)90137-I

Kasting, J. F., & Ackerman, T. P. (1986). Climatic consequences of very high carbon dioxide levels in the Earth's early atmosphere. *Science*, *234*(4782), 1383–1385. https://doi.org/10.1126/science.11539665

Kasting, J. F., & Donahue, T. M. (1980). The evolution of the atmospheric ozone. *Journal of Geophysical Research*, *85*(C6), 3255–3263. https://doi.org/10.1029/JC085iC06p03255

Kennett, J. P., & Stott, L. D. (1991). Abrupt deep-sea warming, palaeoceanographic changes and benthic extinction at the end of the Palaeocene. *Nature*, *353*(6341), 225–229. https://doi.org/10.1038/353225a0

Kidder, D. L., & Worsley, T. R. (2004). Causes and consequences of extreme Permo-Triassic warming to globally equable climate and relation to the Permo-Triassic extinction and recovery. *Palaeogeography, Palaeoclimatology, Palaeoecology*, *203*, 207–237.

Knauth, L. P., & Lowe, D. R. (2003). High Archean climatic temperature inferred from oxygen isotope geochemistry of the cherts in the 3.5 Ga Swaziland Supergroup, South Africa. *Geological Society of America Bulletin*, *115*, 566–580. https://doi.org/10.1130/0016-7606(2003)115<0566:HACTIF>2.0.CO;2

Koch, P. L., Zachos, J. C., & Gingerich, P. D. (1992). Correlation between isotope records in marine and continental carbon reservoirs near the Paleocene/Eocene boundary. *Nature*, *358*, 319–322.

Lary, D. J. (1997). Catalytic destruction of stratospheric ozone. *Journal of Geophysical Research*, *102*(D17), 21,515–21,526. https://doi.org/10.1029/97JD00912

Lebonnois, S., Covey, C., Grossman, A., Parish, H., Schubert, G., et al. (2012). Angular momentum budget in general circulation models of superrotating atmospheres: A critical diagnostic. *Journal of Geophysical Research*, *117*, E12004.

Leconte, J., Forget, F., Charnay, B., Wordsworth, R., & Pottier, A. (2013). Increased insolation threshold for runaway greenhouse process on Earth-like planets. *Nature*, *504*(7479), 268–271. https://doi.org/10.1038/nature12827

Lin, S. J., & Rood, R. B. (1996). Multidimensional flux-form semi-Langrangian transport schemes. *Monthly Weather Review*, *124*(9), 2046–2070. https://doi.org/10.1175/1520-0493(1996)124<2046:MFFSLT>2.0.CO;2

Marty, B., Zimmermann, I., Pujol, L., Burgess, M., & Philippot, P. (2013). Nitrogen isotopic composition and density of the Archean atmosphere. *Science*, *342*, 101–104.

Meraner, K., Mauritsen, T., & Voigt, A. (2013). Robust increase in equilibrium climate sensitivity under global warming. *Geophysical Research Letters*, *40*, 5944–5948. https://doi.org/10.1002/2013GL058118

Neale, R. B., Richter, J. H., Conley, A. J., Park, S., Lauritzen, P. H., Gettelman, A., et al. (2010). Description of the NCAR Community Atmosphere Model (CAM 4.0), NCAR/TN-485+STR NCAR TECHNICAL NOTE.

Petit, J. R., Jouzel, J., Raynaud, D., Barkov, N. I., Barnola, J.-M., Basile, I., Bender, M., et al. (1999). Climate and atmospheric history of the past 420,000 years from the Vostok ice core, Antarctica. *Nature*, *399*(6735), 429–436. https://doi.org/10.1038/20859

Pierrehumbert, R. T., Abbot, D. S., Voigt, A., & Koll, D. (2011). Climate of the Neoproterozoic. *Annual Review of Earth and Planetary Sciences*, *39*(1), 417–460. https://doi.org/10.1146/annurev-earth-040809-152447

Popp, M., Schmidt, H., Marotzke, J., & J. (2016). Transition to a moist greenhouse with CO_2 and solar forcing. *Nature Communications*, *7*, 10,627. https://doi.org/10.1038/ncomms10627

Poulsen, C. J., Jacob, R. L., Pierrehumbert, R. T., & Huynh, T. T. (2002). Testing paleographic controls on a Neoproterozoic snowball Earth. *Geophysical Research Letters*, *29*(11), 1515. https://doi.org/10.1029/2001GL014352

Ramirez, R. M., Kopparapu, R.k., Lindner, V., & Kasting, J. F. (2014). Can increased atmospheric CO_2 levels trigger a runaway greenhouse? *Astrobiology*, *14*(8), 714–731. https://doi.org/10.1089/ast.2014.1153

Ribas, I. (2009). The Sun and stars as the primary energy input in planetary atmospheres. Solar and stellar variability (IAU S264): Impact on Earth and planets. *Proceedings of the International Astronomical Union*, *5*(S264), 3–18. https://doi.org/10.1017/S1743921309992298

Robert, F., & Chaussidon, M. (2006). A paleotemperature curve for the Precambrian oceans based on silicon isotopes in cherts. *Nature*, *443*(7114), 969–972. https://doi.org/10.1038/nature05239

Rogelj, J., Meinshausen, M., & Knutti, R. (2012). Global warming under old and new scenarios using IPCC climate sensitivity range estimates. *Nature Climate*, *2*(4), 248–253. https://doi.org/10.1038/NCLIMATE1385

Rose, B. E. J., & Ferreira, D. (2013). Ocean heat transport and water vapor greenhouse in a warm equable climate: A new look at low gradient paradox. *Journal of Climate*, *26*(6), 2117–2136. https://doi.org/10.1175/JCLI-D-11-00547.1

Rosing, M. T., Bird, D. K., Sleep, N. H., & Bjerrum, C. J. (2010). No climate paradox under the faint early Sun. *Nature*, *464*, 744–749.

Russell, G. L., Lacis, A. A., Rind, D. H., Colose, C., & Opstbaum, R. F. (2013). Fast atmospheric-ocean model runs with large changes in CO_2. *Geophysical Research Letters*, *40*, 5787–5792. https://doi.org/10.1002/2013GL056755

Rye, R., Kuo, P. H., & Holland, H. D. (1995). Atmospheric carbon dioxide concentrations before 2.2 billion years ago. *Nature*, *378*(6557), 603–605. https://doi.org/10.1038/378603a0

Schroder, K.-P., & Smith, R. C. (2008). Distant future of the Sun and Earth revisited. *Monthly Notices of the Royal Astronomical Society*, *386*(1), 155–163. https://doi.org/10.1111/j.1365-2966.2008.13022.x

Shaffer, G., Huber, M., Rondanellii, R., & Pepke Pedersen, J. O. (2016). Deep time evidence for climate sensitivity increase with warming. *Geophysical Research Letters*, *43*, 6538–6545. https://doi.org/10.1002/2016GL069243

Sheldon, N. D. (2006). Precambrian paleosols and atmospheric CO_2 levels. *Precambrian Research*, *147*(1-2), 148–155. https://doi.org/10.1016/j.precamres.2006.02.004

Sherwood, S. C., & Huber, M. (2010). An adaptability limit to climate change due to hear stress. *PNAS*, *107*(21), 9552–9555. https://doi.org/10.1073/pnas.0913352107

Soden, B. J., Held, I. M., Colman, M. R., Shell, K. M., Kiehl, J. T., & Shields, C. (2008). Quantifying climate feedbacks using radiative kernels. *Journal of Climate*, *21*(14), 3504–3520. https://doi.org/10.1175/2007JCLI2110.1

Som, S. M., Catling, D. C., Harnmeijer, J. P., Polivka, P. M., & Buick, R. (2012). Air density 2.7 billion years ago limited to less than twice modern levels by fossil raindrop imprints. *Nature*, *484*(7394), 359–362. https://doi.org/10.1038/nature10890

Sundquist, E. T. (1991). Steady- and non-steady-state carbonate-silicate controls on atmospheric CO_2. *Quaternary Science Reviews*, *10*(2-3), 283–296. https://doi.org/10.1016/0277-3791(91)90026-Q

Towe, K. M. (1981). Environmental conditions surrounding the origin and early evolution of life: A hypothesis. *Precambrian Research*, *16*(1-2), 1–10. https://doi.org/10.1016/0301-9268(81)90002-4

Walker, J. C. G., Hays, P. B., & Kasting, J. F. (1981). A negative feedback mechanisms for the long-term stabilizations of Earth's surface temperature. *Journal of Geophysical Research*, *86*(C10), 9776–9782. https://doi.org/10.1029/JC086iC10p09776

Wolf, E. T., & Toon, O. B. (2013). Hospitable Archean climates simulated by a general circulation model. *Astrobiology*, *13*(7), 656–673. https://doi.org/10.1089/ast.2012.0936

Wolf, E. T., & Toon, O. B. (2014). Controls on the Archean climate system investigated with a global climate model. *Astrobiology*, *41*(1), 167–172. https://doi.org/10.1002/2013GL058376

Wolf, E. T., & Toon, O. B. (2015). The evolution of habitable climates under the brightening Sun. *Journal of Geophysical Research: Atmospheres*, *120*, 5775–5794. https://doi.org/10.1002/2015JD023302